Optimum Design of a Three-Axis Magnetic Field Simulator

M. PASTENA

M. GRASSI
University of Naples "Federico II"
Italy

This paper deals with the design of a three-axis magnetic field simulator for space applications. The simulator main goal is to reproduce, in an assigned volume about its geometrical center, a magnetic field vector with assigned uniformity and time behavior. To this end, different geometrical configurations, in terms of coil shape, dimension, number and distance, are analyzed. Results show that an optimum configuration, in terms of test volume dimensions and maximum power consumption, can be found.

Manuscript received January 19, 2001; revised October 23, 2001; released for publication January 16, 2002.

IEEE Log No. T-AES/38/2/11437.

Refereeing of this contribution was handled by T. E. Busch.

This work was supported by the Italian Space Agency, the Ministry for University and Scientific and Technological Research, and Regione Campania.

Authors' address: Department of Space Science and Engineering, University of Naples "Federico II", p.le Tecchio 80, I-80125 Napoli, Italy, E-mail: (pastena@unina.it).

I. INTRODUCTION

The magnetic field simulator study is performed in the framework of a joint project between the two Universities of Naples for the development of a satellite integration and ground test laboratory. The laboratory development gets into an educational project, financed by the Italian Space Agency, the Italian Ministry of University and of Technology and Scientific Research and Regione Campania, for the development of the University microsatellite SMART (Scientific Microsatellite for Advanced Research and Technology). This last one is a multimission microsatellite for remote sensing applications in Sun-synchronous orbits [1].

A magnetic field simulator is a system of 6 or more coils mounted with their axes aligned along mutually perpendicular directions. Modulating the coil supply currents makes it possible to reproduce the modulus and direction variation of a magnetic field vector by means of its components along the axes of an orthogonal, right-handed reference frame. Magnetic field simulators have been widely analyzed in the literature. They basically are Helmholtz-coil systems used mainly for magnetometer calibration and test [2, 3]. Nevertheless, in the case of space applications, a magnetic field simulator allows additional ground tests to be performed: magnetic sensor and actuator calibration and functional testing, studies of high-intensity field effects on space components and materials, evaluation of the space vehicle magnetic dipole moment, etc.

Considering the various applications, two basic simulator classes can be identified:

1) high intensity field simulators, in which the main requirement is the maximum value of the magnetic field to be realized in a given test volume;
2) high uniformity field simulators, in which the main requirement is the minimum field variation, with respect to a nominal field, to be realized in a given test volume.

For the above two classes, this report aims at identifying the design critical parameters and at optimizing them in order to find the simulator geometrical configuration which best fits the design requirements. To this end, different geometrical configurations, in terms of coil dimension, number, shape, and distance, are analyzed. In particular, two coil shapes are considered: circular and square coils. The configuration analysis is performed using analytical and numerical models based on a two-coil system geometry. The advantage of using a coil shape with respect to the other is then evaluated by using the maximum power consumption and the test volume dimension (in which a predetermined value of the field uniformity is realized) as parameters.

II. SIMULATOR DESIGN

A. Simulator Design Main Drivers

This work aims at developing design criteria valid for any simulator class. As pointed out before, two main classes can be identified: 1) high intensity field simulators, and 2) high uniformity field simulators.

In the first case, for assigned field uniformity and test volume dimensions (in which the uniformity is realized), high intensity fields can be obtained only by increasing the supply current and/or the coil dimension. In both cases, the maximum power consumption increases. As a consequence, for high intensity field simulators the critical design parameter is the maximum power consumption.

In the second case, for a given magnetic field intensity, improving the uniformity value in an assigned test volume requires the system dimensions to be increased (i.e., coil dimension and distance increase). As a result, in this case, the critical design parameter becomes the ratio between test volume and coil dimension.

In the following, different system geometrical configurations are analyzed considering two coil shapes: circular (identified by the c subscript) and square (identified by the s subscript) coils.

B. Analytical Models and Definitions

If two circular coils, with their axes aligned with the z axis of a cylindrical reference frame, CRF (whose origin is at the geometrical center of the two coils and the z axis is aligned with the coil axis), are supplied with a current I_c, the magnetic field components in the axial (z) and radial (ρ) directions (Fig. 1) are given by the following analytical expressions [4]:

$$B_\rho = \frac{\mu_0 N_c I_c}{4\pi}\left\{\frac{\left(\frac{d_c}{2}+z\right)k_1}{\rho\sqrt{a_c\rho}}\left[-I_1(k_1)+\frac{a_c^2+\rho^2+\left(\frac{d_c}{2}+z\right)^2}{(a_c-\rho)^2+\left(\frac{d_c}{2}+z\right)^2}I_2(k_1)\right]\right.$$
$$\left.-\frac{\left(\frac{d_c}{2}-z\right)k_2}{\rho\sqrt{a\rho}}\left[-I_1(k_2)+\frac{a_c^2+\rho^2+\left(\frac{d_c}{2}-z\right)^2}{(a_c-\rho)^2+\left(\frac{d_c}{2}-z\right)^2}I_2(k_2)\right]\right\} \quad (1)$$

$$B_z = \frac{\mu_0 N_c I_c}{4\pi}\left\{\frac{k_1}{\sqrt{a_c\rho}}\left[I_1(k_1)+\frac{a_c^2-\rho^2-\left(\frac{d_c}{2}+z\right)^2}{(a_c-\rho)^2+\left(\frac{d_c}{2}+z\right)^2}I_2(k_1)\right]+\frac{k_2}{\sqrt{a_c\rho}}\left[I_1(k_2)+\frac{a_c^2-\rho^2-\left(\frac{d_c}{2}-z\right)^2}{(a_c-\rho)^2+\left(\frac{d_c}{2}-z\right)^2}I_2(k_2)\right]\right\}$$

where a_c is the coil radius, N_c is the number of windings of one coil, d_c is the distance between the geometrical centers of the two coils, μ_0 is the vacuum magnetic permeability, and I_1 and I_2 are the fist and second type elliptic integrals, respectively, in which k_1 and k_2 are given by

$$k_1 = \sqrt{\frac{4a_c\rho}{(a_c+\rho)^2+\left(\frac{d_c}{2}+z\right)^2}}$$
$$k_2 = \sqrt{\frac{4a_c\rho}{(a_c+\rho)^2+\left(\frac{d_c}{2}-z\right)^2}}. \quad (2)$$

If two square coils, with their axes aligned with the CRF z axis, are supplied with a current I_s, the magnetic field components in the axial (z) and radial

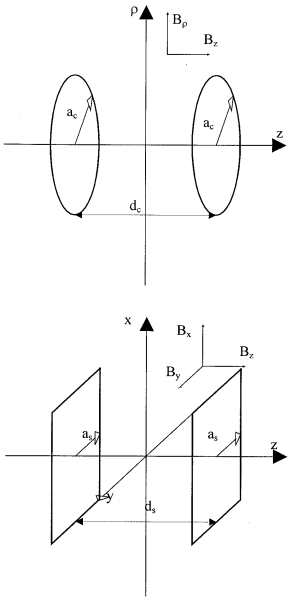

Fig. 1. Two-coil system reference frames.

(x, y) directions (Fig. 1) are given by the following analytical expressions [5]:

$$
\begin{aligned}
B_x = \Bigg\{ \Bigg\{ (a_s - y) \Bigg[& \frac{1}{\left[(a_s - x)^2 + \left(z + \frac{d_s}{2}\right)^2\right] \sqrt{(a_s - y)^2 + (a_s - x)^2 + \left(z + \frac{d_s}{2}\right)^2}} \\
& - \frac{1}{\left[(a_s + x)^2 + \left(z + \frac{d_s}{2}\right)^2\right] \sqrt{(a_s - y)^2 + (a_s + x)^2 + \left(z + \frac{d_s}{2}\right)^2}} \Bigg] \\
+ (a_s + y) \Bigg[& \frac{1}{\left[(a_s - x)^2 + \left(z + \frac{d_s}{2}\right)^2\right] \sqrt{(a_s + y)^2 + (a_s - x)^2 + \left(z + \frac{d_s}{2}\right)^2}} \\
& - \frac{1}{\left[(a_s + x)^2 + \left(z + \frac{d_s}{2}\right)^2\right] \sqrt{(a_s + y)^2 + (a_s + x)^2 + \left(z + \frac{d_s}{2}\right)^2}} \Bigg] \Bigg\} \left(z + \frac{d_s}{2}\right) \\
+ \left(z - \frac{d_s}{2}\right) \Bigg\{ (a_s - y) \Bigg[& \frac{1}{\left[(a_s - x)^2 + \left(z - \frac{d_s}{2}\right)^2\right] \sqrt{(a_s - y)^2 + (a_s - x)^2 + \left(z - \frac{d_s}{2}\right)^2}} \\
& - \frac{1}{\left[(a_s + x)^2 + \left(z - \frac{d_s}{2}\right)^2\right] \sqrt{(a_s - y)^2 + (a_s + x)^2 + \left(z - \frac{d_s}{2}\right)^2}} \Bigg] \\
+ (a_s + y) \Bigg[& \frac{1}{\left[(a_s - x)^2 + \left(z - \frac{d_s}{2}\right)^2\right] \sqrt{(a_s + y)^2 + (a_s - x)^2 + \left(z - \frac{d_s}{2}\right)^2}} \\
& - \frac{1}{\left[(a_s + x)^2 + \left(z - \frac{d_s}{2}\right)^2\right] \sqrt{(a_s + y)^2 + (a_s + x)^2 + \left(z - \frac{d_s}{2}\right)^2}} \Bigg] \Bigg\} \Bigg\} \frac{\mu_0 N_s I_s}{4\pi}
\end{aligned}
\tag{3a}
$$

$$
\begin{aligned}
B_y = \Bigg\{ \Bigg\{ (a_s - x) \Bigg[& \frac{1}{\left[(a_s-y)^2 + \left(z+\frac{d_s}{2}\right)^2\right]\sqrt{(a_s-x)^2+(a_s-y)^2+\left(z+\frac{d_s}{2}\right)^2}} \\
& - \frac{1}{\left[(a_s+y)^2 + \left(z+\frac{d_s}{2}\right)^2\right]\sqrt{(a_s-x)^2+(a_s+y)^2+\left(z+\frac{d_s}{2}\right)^2}} \Bigg] \\
+ (a_s + x) \Bigg[& \frac{1}{\left[(a_s-y)^2 + \left(z+\frac{d_s}{2}\right)^2\right]\sqrt{(a_s+x)^2+(a_s-y)^2+\left(z+\frac{d_s}{2}\right)^2}} \\
& - \frac{1}{\left[(a_s+y)^2 + \left(z+\frac{d_s}{2}\right)^2\right]\sqrt{(a_s+x)^2+(a_s+y)^2+\left(z+\frac{d_s}{2}\right)^2}} \Bigg] \Bigg\} \left(z+\frac{d_s}{2}\right) \\
+ \left(z-\frac{d_s}{2}\right) \Bigg\{ (a_s - x) \Bigg[& \frac{1}{\left[(a_s-y)^2 + \left(z-\frac{d_s}{2}\right)^2\right]\sqrt{(a_s-x)^2+(a_s-y)^2+\left(z-\frac{d_s}{2}\right)^2}} \\
& - \frac{1}{\left[(a_s+y)^2 + \left(z-\frac{d_s}{2}\right)^2\right]\sqrt{(a_s-x)^2+(a_s+y)^2+\left(z-\frac{d_s}{2}\right)^2}} \Bigg] \\
+ (a_s + x) \Bigg[& \frac{1}{\left[(a_s-y)^2 + \left(z-\frac{d_s}{2}\right)^2\right]\sqrt{(a_s+x)^2+(a_s-y)^2+\left(z-\frac{d_s}{2}\right)^2}} \\
& - \frac{1}{\left[(a_s+y)^2 + \left(z-\frac{d_s}{2}\right)^2\right]\sqrt{(a_s+x)^2+(a_s+y)^2+\left(z-\frac{d_s}{2}\right)^2}} \Bigg] \Bigg\} \Bigg) \frac{\mu_0 N_s I_s}{4\pi}
\end{aligned}
\tag{3b}
$$

$$
\begin{aligned}
B_Z = \Bigg\{ & \frac{(a_s-x)(a_s-y)}{\sqrt{(a_s-x)^2+(a_s-y)^2+\left(z+\frac{d_s}{2}\right)^2}}\left[\frac{1}{\left[(a_s-x)^2+\left(z+\frac{d_s}{2}\right)^2\right]}+\frac{1}{\left[(a_s-y)^2+\left(z+\frac{d_s}{2}\right)^2\right]}\right] \\
& + \frac{(a_s-x)(a_s+y)}{\sqrt{(a_s-x)^2+(a_s+y)^2+\left(z+\frac{d_s}{2}\right)^2}}\left[\frac{1}{\left[(a_s-x)^2+\left(z+\frac{d_s}{2}\right)^2\right]}+\frac{1}{\left[(a_s+y)^2+\left(z+\frac{d_s}{2}\right)^2\right]}\right] \\
& + \frac{(a_s+x)(a_s-y)}{\sqrt{(a_s+x)^2+(a_s-y)^2+\left(z+\frac{d_s}{2}\right)^2}}\left[\frac{1}{\left[(a_s+x)^2+\left(z+\frac{d_s}{2}\right)^2\right]}+\frac{1}{\left[(a_s-y)^2+\left(z+\frac{d_s}{2}\right)^2\right]}\right] \\
& + \frac{(a_s+x)(a_s+y)}{\sqrt{(a_s+x)^2+(a_s+y)^2+\left(z+\frac{d_s}{2}\right)^2}}\left[\frac{1}{\left[(a_s+x)^2+\left(z+\frac{d_s}{2}\right)^2\right]}+\frac{1}{\left[(a_s+y)^2+\left(z+\frac{d_s}{2}\right)^2\right]}\right] \\
& + \frac{(a_s-x)(a_s-y)}{\sqrt{(a_s-x)^2+(a_s-y)^2+\left(z-\frac{d_s}{2}\right)^2}}\left[\frac{1}{\left[(a_s-x)^2+\left(z+\frac{d_s}{2}\right)^2\right]}+\frac{1}{\left[(a_s-y)^2+\left(z-\frac{d_s}{2}\right)^2\right]}\right] \\
& + \frac{(a_s-x)(a_s+y)}{\sqrt{(a_s-x)^2+(a_s+y)^2+\left(z-\frac{d_s}{2}\right)^2}}\left[\frac{1}{\left[(a_s-x)^2+\left(z-\frac{d_s}{2}\right)^2\right]}+\frac{1}{\left[(a_s+y)^2+\left(z-\frac{d_s}{2}\right)^2\right]}\right] \\
& + \frac{(a_s+x)(a_s-y)}{\sqrt{(a_s+x)^2+(a_s-y)^2+\left(z-\frac{d_s}{2}\right)^2}}\left[\frac{1}{\left[(a_s+x)^2+\left(z-\frac{d_s}{2}\right)^2\right]}+\frac{1}{\left[(a_s-y)^2+\left(z-\frac{d_s}{2}\right)^2\right]}\right] \\
& + \frac{(a_s+x)(a_s+y)}{\sqrt{(a_s+x)^2+(a_s+y)^2+\left(z-\frac{d_s}{2}\right)^2}}\left[\frac{1}{\left[(a_s+x)^2+\left(z+\frac{d_s}{2}\right)^2\right]}+\frac{1}{\left[(a_s+y)^2+\left(z-\frac{d_s}{2}\right)^2\right]}\right]\Bigg\}\frac{\mu_0 N_s I_s}{4\pi}
\end{aligned}
\tag{3c}
$$

where $2a_s$ is the coil side dimension, N_s is the number of windings of one coil, d_s is the distance between the geometrical centers of the two coils, and I_s is the supply current. Equations (1), (3a), (3b), and (3c) show that, independent of the coil shape, at the CRF origin only the z-axis component of the magnetic field vector is non zero and it is given by the following analytical expression:

$$B_z(0,0) = \frac{\mu_0 N_c I_c a_c^2}{\left[\left(\frac{d_c}{2}\right)^2 + a_c^2\right]^{3/2}} = B_c(d_c, a_c)$$

for circular coils (4a)

$$B_z(0,0,0) = \frac{\mu_0 N_s I_s 4a_s^2}{\left[\left(\frac{d_s}{2}\right)^2 + a_s^2\right]\sqrt{2a_s^2 + \left(\frac{d_s}{2}\right)^2}} = B_s(d_s, a_s)$$

for square coils (4b)

where $B_c(B_s)$ is the field vector modulus for circular (square) coils. In addition, at the CRF origin the first derivative of the magnetic field vector modulus with respect to z is zero, independent of the two-coil system geometry.

The field vector uniformity is defined as the field deviation, in modulus and direction, with respect to the nominal field, which is taken coincident with the one evaluated at the test volume geometrical center (i.e., at the CRF origin). Therefore, the field uniformity is modeled by two functions: the modulus percentage error e_M, which is the field modulus deviation evaluated as a percentage of the nominal field modulus, and the direction error e_A. The modulus percentage and direction errors of the magnetic field vector, evaluated at a point of CRF, are then given by the following analytical expressions:

$$\begin{aligned}
e_{Mc}\left(\frac{z}{a_c}, \frac{\rho}{a_c}, \frac{d_c}{a_c}\right) &= 100 - \frac{B(z,\rho,d_c,a_c)}{B_{\text{nom}c}(d_c,a_c)} \cdot 100 \\
e_{Ms}\left(\frac{x}{a_s}, \frac{y}{a_s}, \frac{z}{a_s}, \frac{d_s}{a_s}\right) &= 100 - \frac{B(x,y,z,d_s,a_s)}{B_{\text{nom}s}(d_s,a_s)} \cdot 100 \\
e_{Ac}\left(\frac{z}{a_c}, \frac{\rho}{a_c}, \frac{d_c}{a_c}\right) &= \text{arctn}\left(\frac{B_\rho(z,\rho,d_c,a_c)}{B_Z(z,\rho,d_c,a_c)}\right) \qquad (5) \\
e_{As}\left(\frac{x}{a_s}, \frac{y}{a_s}, \frac{z}{a_s}, \frac{d_s}{a_s}\right) & \\
&= \text{arctn}\left(\frac{\sqrt{B_x^2(x,y,z,d_s,a_s) + B_y^2(x,y,z,d_s,a_s)}}{B_Z(x,y,z,d_s,a_s)}\right)
\end{aligned}$$

where B is the modulus of the magnetic field vector at the considered point and the subscript nom indicates nominal field. It is worth noting that the values of e_{Mc} and e_{Ac} (e_{Ms} and e_{As}) depend only on d_c/a_c (d_s/a_s).

III. SEARCHING FOR THE OPTIMUM GEOMETRICAL CONFIGURATION

A. Helmholtz-Coil Configuration

It is well known from the literature [5] that the Helmholtz-coil configuration minimizes the field vector modulus variation in the axial direction (z axis), i.e., it is the one in which d/a is selected so that the second derivative of the field vector modulus with respect to z, evaluated at the CRF origin, is equal to zero. After some mathematics, from (1)–(3) it is possible to obtain the value of d/a corresponding to the Helmholtz coil configuration for circular and square coils:

$$\frac{d_c}{a_c} = 1 \qquad (6a)$$

$$\frac{d_s}{a_s} = \sqrt{\sqrt[3]{\frac{64}{3} + \frac{16}{27}\sqrt{610}} + \sqrt[3]{\frac{64}{3} - \frac{16}{27}\sqrt{610}} - 4} \approx 1.089011. \qquad (6b)$$

Figs. 2(a) to 3(b) show the contour plots of e_{Mc}, e_{Ac}, e_{Ms}, and e_{As}, evaluated for a pair of coils in

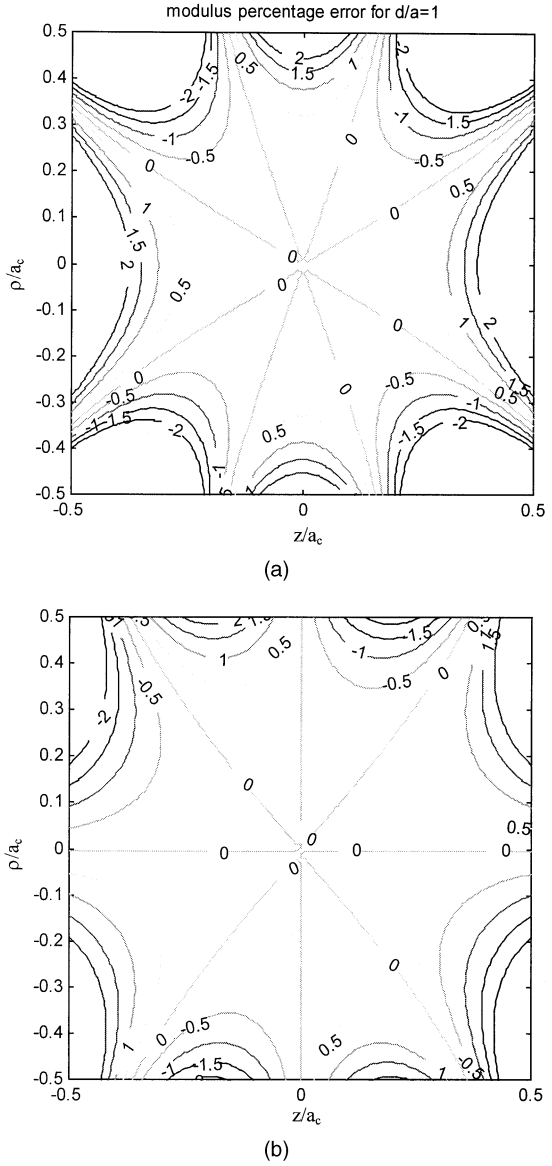

Fig. 2. Modulus percentage (a) and direction errors (b) for Helmholtz configuration (circular coils).

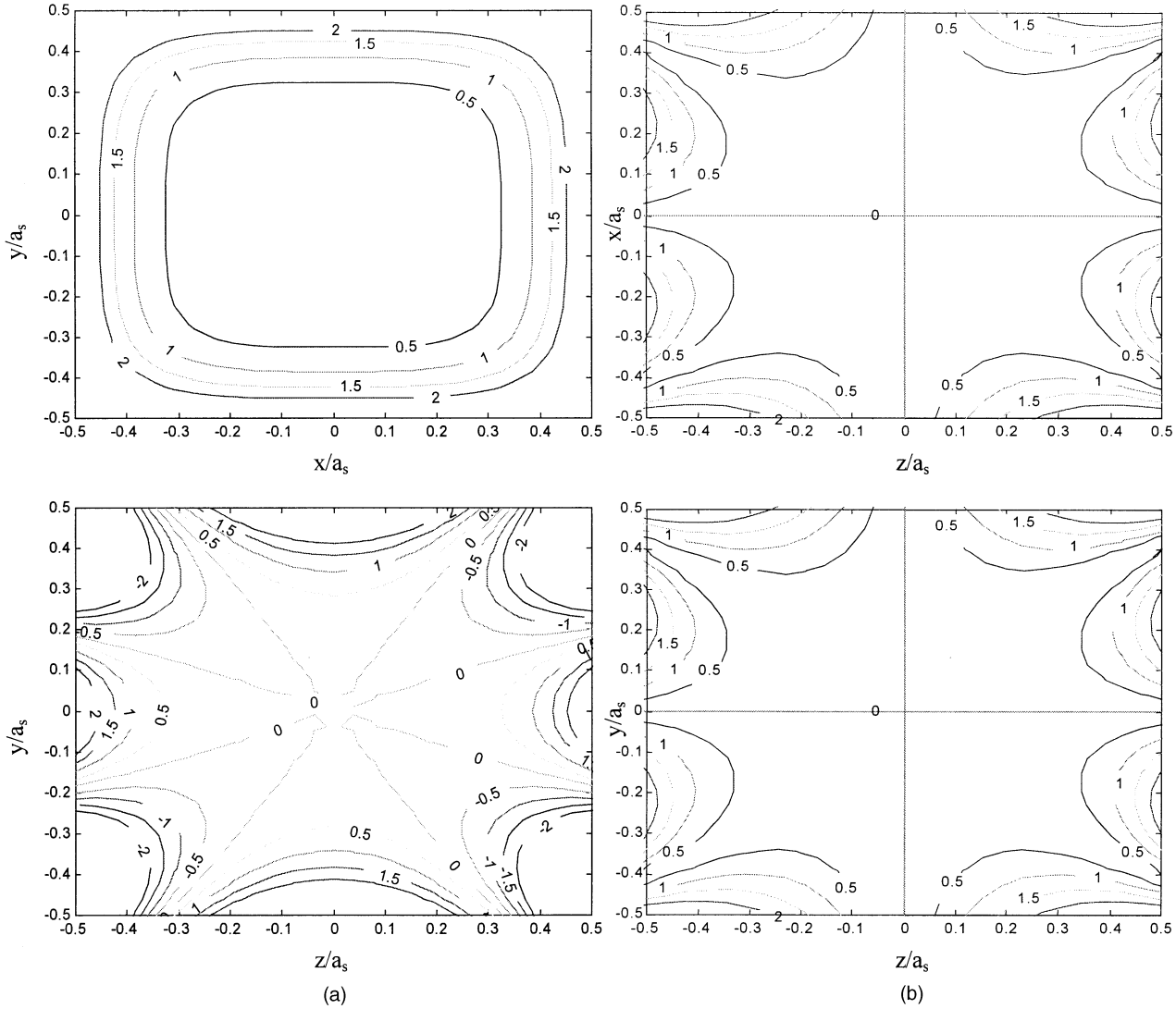

Fig. 3. Modulus percentage and direction errors for Helmholtz configuration (square coils).

the Helmholtz configuration (i.e., for $d_c/a_c = 1$ and $d_s/a_s = 1.089011$, respectively). These contour plots allow the uniformity volume boundaries for different uniformity percentage values to be identified. Considering the typical resolution of three-axis fluxgate magnetometers for satellite attitude determination (1 mG) [2–3], field modulus variations lower than 1% cannot be detected. As a consequence, a 1% uniformity value is considered in the following for discussion of the results. It is possible to see that the 1% uniformity volume axial dimension is smaller than the radial one, both for circular and square coils. Since the uniformity volume of the simulator is given by the intersection of the uniformity volumes of the three couples of coils, if the Helmholtz-configuration is used, the simulator 1% uniformity volume is smaller than the one of a single pair of coils (Fig. 4). This is because the dimension of the 1% uniformity volume along each CRF axis is the smallest between the axial and the radial dimensions of the 1% uniformity volume of a single pair of coils.

Since, in our case, the main design objective is to maximize the test volume dimensions in which a predetermined value of the magnetic field vector uniformity is realized, in the following a different system configuration is analyzed.

B. Optimum Configuration

For a single pair of coils, the uniformity volume dimension in the axial and radial directions can be calculated by equaling the error function $e_{Mc}(e_{Ms})$, evaluated for $\rho = 0$ and $z = 0$, respectively ($x = y = 0$, $y = z = 0$, and $x = z = 0$, respectively), to the uniformity percentage design value. Since $e_{Mc}(e_{Ms})$ is a function of z/a_c, ρ/a_c, and d_c/a_c (z/a_s, x/a_s, y/a_s, and d_s/a_s), the uniformity volume dimension, as a percentile of the coil radius, depends only on d_c/a_c (d_s/a_s). Therefore, substituting in turn $\rho = 0$ and $z = 0$ ($x = y = 0$, $z = y = 0$, and $z = x = 0$), in the first

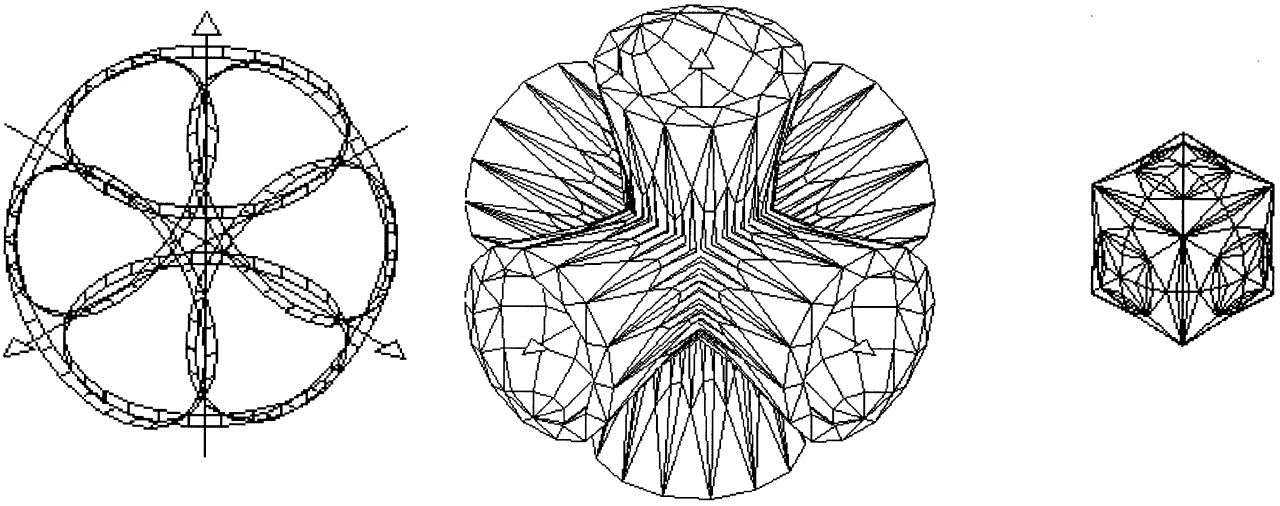

Fig. 4. Six-coil system and resulting test volume. (a) Coil positioning. (b) Uniformity volumes. (c) Resulting test volume.

of equations (5) (in the second of equations (5)), it follows that

$$e_{Mc}\left(\frac{z}{a_c},\frac{d_c}{a}\right)\Big|_{\rho=0} = 100 - \frac{B(z,a_c,d_c)|_{\rho=0}}{B_{\mathrm{nom}c}(a_c,d_c)}100 \tag{7a}$$

$$e_{Mc}\left(\frac{\rho}{a_c},\frac{d_c}{a_c}\right)\Big|_{z=0} = 100 - \frac{B(\rho,a_c,d_c)|_{z=0}}{B_{\mathrm{nom}c}(a_c,d_c)}100 \tag{7b}$$

$$e_{Ms}\left(\frac{z}{a_s},\frac{d_s}{a_s}\right)\Big|_{x=0,y=0} = 100 - \frac{B(z,a_s,d_s)|_{x=0,y=0}}{B_{\mathrm{nom}s}(a_s,d_s)}100 \tag{7c}$$

$$e_{Ms}\left(\frac{x}{a_s},\frac{d_s}{a_s}\right)\Big|_{z=0,y=0} = 100 - \frac{B(z,a_s,d_s)|_{z=0,y=0}}{B_{\mathrm{nom}s}(a_s,d_s)}100 \tag{7d}$$

$$e_{Ms}\left(\frac{y}{a_s},\frac{d_s}{a_s}\right)\Big|_{x=0,z=0} = 100 - \frac{B(z,a_s,d_s)|_{x=0,z=0}}{B_{\mathrm{nom}s}(a_s,d_s)}100. \tag{7e}$$

It is worth noting that from (3a), (3b), (7d), and (7e) it follows that

$$e_{Ms}\left(\frac{x}{a_s},\frac{d_s}{a_s}\right)\Big|_{z=0,y=0} = e_{Ms}\left(\frac{y}{a_s},\frac{d_s}{a_s}\right)\Big|_{z=0,x=0}. \tag{8}$$

Equation (8) states that in the case of square coils the uniformity volume dimensions along the x and y axes are equal, independently on the value of d_s/a_s.

Figs. 5(a) and 5(b) show, respectively, the contour plots of e_{Mc} and e_{Ms} versus d/a along the axial and radial directions, as well as the position of the centers of the two coils in the axial direction (i.e., $z = d/2$ and $z = -d/2$). Fig. 5 allows the behavior of the uniformity volume axial and radial dimensions as a function of d/a to be visualized. In the case of circular coils, it is possible to see that selecting d_c/a_c equal to 1.116 (0.869) maximizes the 1% uniformity volume axial (radial) dimension.

The simulator uniformity volume dimension along each CRF axis is equal to the smallest between the axial and radial dimensions of the uniformity volume of a single pair of coils. As a consequence, the value of d/a that maximizes the simulator uniformity volume, for a given coil dimension, is the one that makes equal the axial and radial dimensions of the uniformity volume of a single pair of coils. Therefore, the simulator uniformity volume includes a spherical test volume with a maximum radius equal to the axial dimension of the two-coil system uniformity volume. Fig. 6 shows the behavior of the optimum value of d/a as a function of the uniformity percentage design value. It is worth noting that when the uniformity percentage value tends to zero the optimum value of d/a tends to the Helmholtz configuration one. Fig. 7 shows the behavior of the test volume radius, as a percentile of the coil dimension, versus the uniformity percentage design value. Fig. 8 shows the gain in the test volume radius given by the use of the optimum configuration instead of the Helmholtz one, as a function of the uniformity percentage design value for circular and square coils. It is worth noting that, for a given coil dimension, if uniformity percentage values less than 1% are required, the use of the optimum configuration allows a test volume radius gain greater than 10%, in the case of circular coils, and greater than 6%, in the case of square coils.

C. Optimum Configuration Effects on Field Accuracy

The value of the nominal field modulus produced by the ith pair of coils, in the optimum configuration, is given by the following analytical expression:

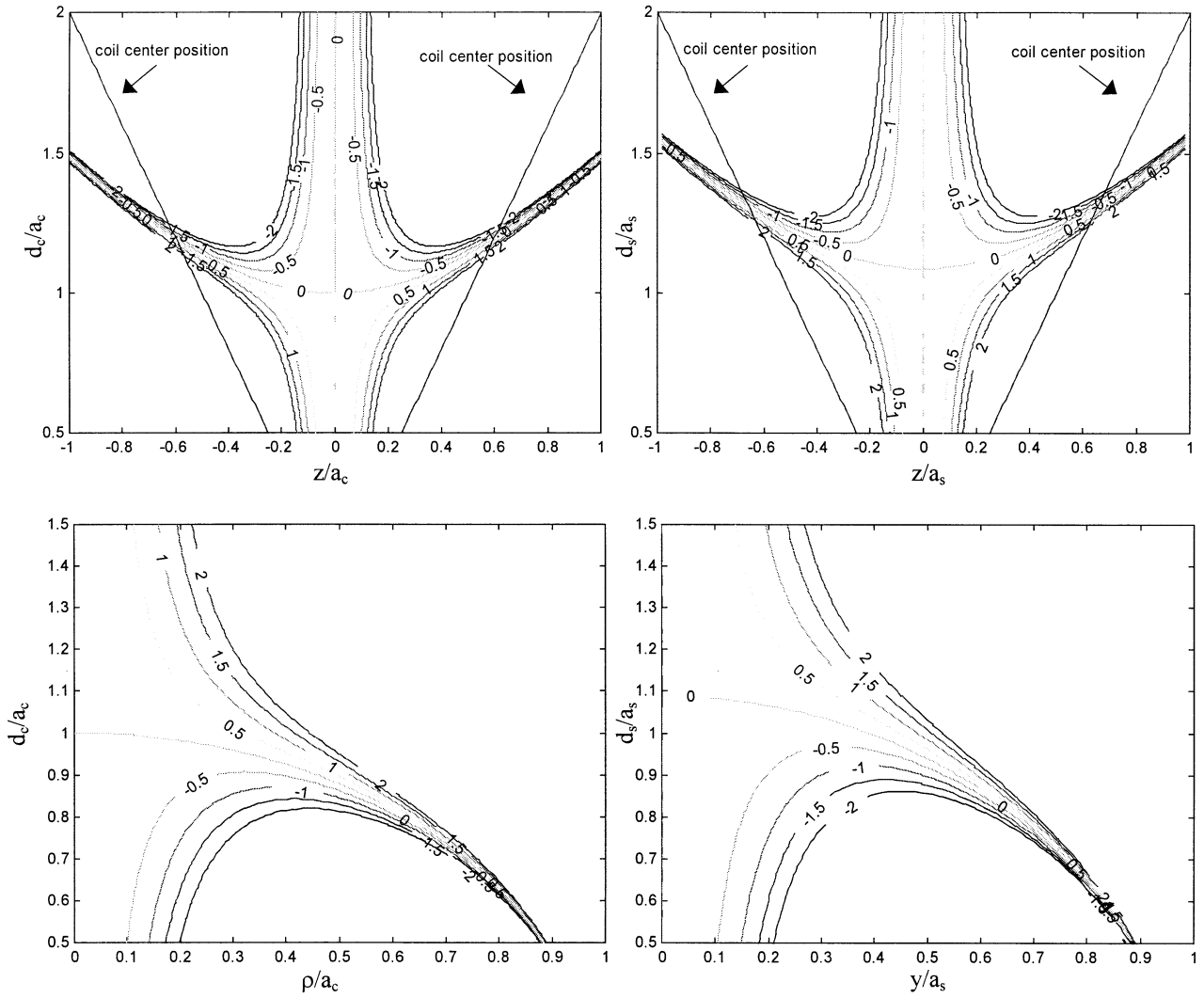

Fig. 5. Contour plots of modulus percentage error for various values of d/a.

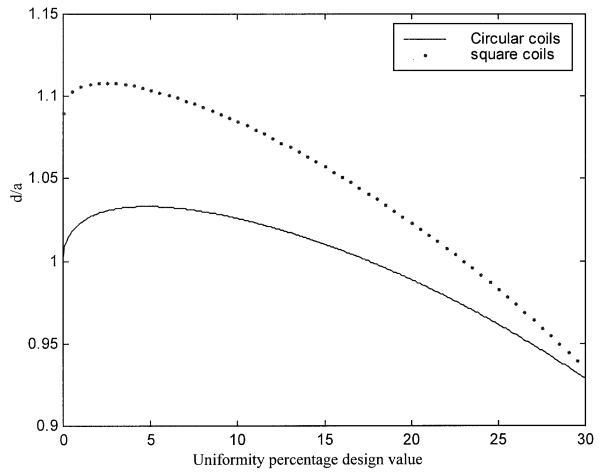

Fig. 6. Optimum d/a versus uniformity percentage design value.

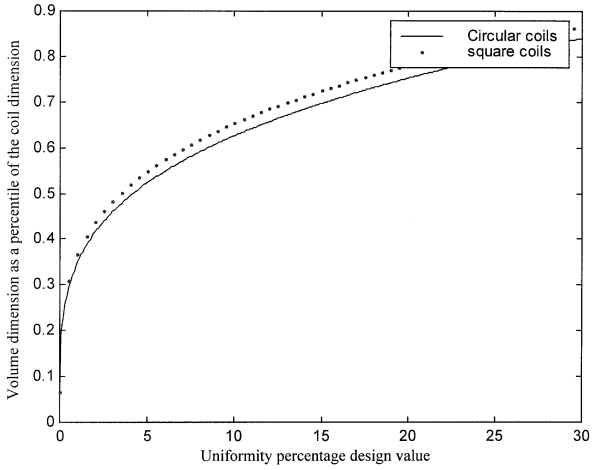

Fig. 7. Test volume dimension as percentile of coil dimension versus uniformity design value.

$$B_{ci} = \frac{\mu_0}{a_{ci}\left[\frac{1}{4}\left(\frac{d_c}{a_c}\right)^2_{\text{opt}} + 1\right]^{3/2}} N_{ci} I_{ci} \quad \text{for circular coils} \qquad (9a)$$

$$B_{si} = \frac{\mu_0 4}{a_{si}\left[\frac{1}{4}\left(\frac{d_s}{a_s}\right)^2_{\text{opt}} + 1\right]\sqrt{2 + \frac{1}{4}\left(\frac{d_s}{a_s}\right)^2_{\text{opt}}}} N_{si} I_{si} \quad \text{for square coils} \qquad (9b)$$

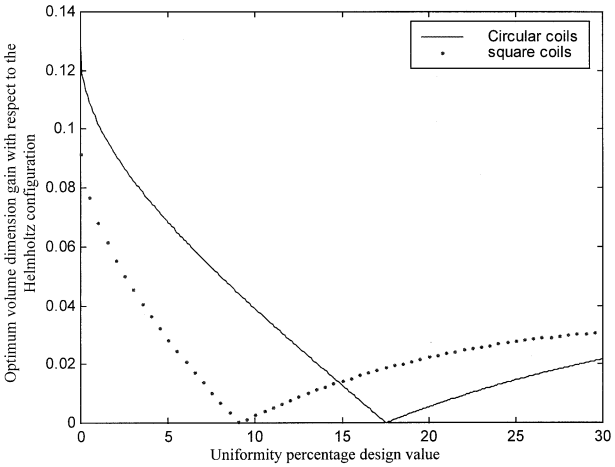

Fig. 8. Test volume dimension gain with respect to Helmholtz configuration versus uniformity design value.

where the i subscript indicates the ith pair of coils. If three identical pairs of coils are used for the simulator, (9a) and (9b) can be rewritten as follows:

$$G_{\mathrm{opt}c}B_{ci} = N_c I_{ci} \tag{10a}$$

$$G_{\mathrm{opt}s}B_{si} = N_s I_{si} \tag{10b}$$

where $G_{\mathrm{opt}c}$ and $G_{\mathrm{opt}s}$ are the optimum values of the coil geometrical parameters given by the following analytical expressions:

$$G_c = \frac{\left[\frac{1}{4}\left(\frac{d_c}{a_c}\right)^2 + 1\right]^{3/2}}{\mathrm{scf}_c \mu_0} r_{tvc} \tag{11a}$$

$$G_s = \frac{\left[\frac{1}{4}\left(\frac{d_s}{a_s}\right)^2 + 1\right]\sqrt{2 + \frac{1}{4}\left(\frac{d_s}{a_s}\right)^2}}{4\mathrm{scf}_s \mu_0} r_{tvs}. \tag{11b}$$

In the previous equations scf is the scale factor:

$$\begin{aligned} \mathrm{scf}_c &= \frac{r_{tvc}}{a_c} \\ \mathrm{scf}_c &= \frac{r_{tvs}}{a_s}. \end{aligned} \tag{12}$$

It can be observed that the scale factors $\mathrm{scf}_c(\mathrm{scf}_s)$ depends only on $d_c/a_c(d_s/a_s)$, whereas the geometrical parameter $G_c(G_s)$ depends on both d_c/a_c and the test volume radius r_{tvc} (d_s/a_s and r_{tvs}).

Considering that, for given coil dimension and distance, the maximum value of the nominal magnetic field ith component is obtained for the maximum value of the supply current, the number of windings for each coil can be evaluated as follows:

$$N_c = \frac{B_{ci\max} \cdot G_{\mathrm{opt}c}}{I_{ci\max}} \tag{13a}$$

$$N_s = \frac{B_{si\max} \cdot G_{\mathrm{opt}s}}{I_{si\max}}. \tag{13b}$$

The standard deviation in the nominal magnetic field ith component can be then calculated from (10a) and (10b) as follows [6]:

$$\sigma_{B_{ci}} = \left(\frac{N_c}{G_{\mathrm{opt}c}}\right)\sigma_{I_{ci}} \tag{14a}$$

$$\sigma_{B_{si}} = \left(\frac{N_s}{G_{\mathrm{opt}s}}\right)\sigma_{I_{si}} \tag{14b}$$

where $\sigma_{I_{ic}}$ and $\sigma_{I_{is}}$ are the supply current standard deviations [7]. Substituting (13a) and (14a) into (13b) and (14b), respectively, it follows that

$$\sigma_{B_{ci}} = \left(\frac{B_{c\max}}{I_{c\max}}\right)\sigma_{I_{ci}} \tag{15a}$$

$$\sigma_{B_{si}} = \left(\frac{B_{s\max}}{I_{s\max}}\right)\sigma_{I_{si}}. \tag{15b}$$

Equations (15a) and (15b) state that the error in the nominal field ith component does not depend on the value of G_c and G_s, and, consequently, on the selected system configuration. On the contrary, it depends on both the uncertainty and the maximum value of the supply currents. Therefore, these parameters become the key parameters for the selection of the power supply for the simulator.

D. Optimum Configuration Effects on Power Consumption

The selected configuration is optimum also in terms of power consumption. In fact, for each pair of coils, the coil resistance can be expressed as follows:

$$R_c = \frac{4\pi a_c N_c}{s}\rho_m \tag{16a}$$

$$R_s = \frac{16 a_s N_s}{s}\rho_m \tag{16b}$$

where s is the coil wire section, whose selection depends on the maximum value of the supply current, and ρ_m is the wire electrical resistivity. Using (13a), (13b), (16a), and (16b) the maximum power consumption for the ith pair of coils can be expressed as follows:

$$P_{ci\max} = R_c I_{ci\max}^2 = \frac{\rho_m 4\pi a_c G_c B_{ci\max} I_{ci\max}}{s} \tag{17a}$$

$$P_{si\max} = R_s I_{si\max}^2 = \frac{\rho_m 16 a_s G_s B_{si\max} I_{si\max}}{s}. \tag{17b}$$

Therefore, the maximum power consumption depends on the selected configuration. Substituting (11a) and (11b) into (17a) and (17b), it follows that

$$P_{ci\max} = \frac{\rho_m 4\pi B_{ci\max} I_{ci\max}}{s} \frac{\left[\frac{1}{4}\left(\frac{d_c}{a_c}\right)^2 + 1\right]^{3/2}}{\mathrm{scf}_c^2 \mu_0} r_{tvc}^2 \tag{18a}$$

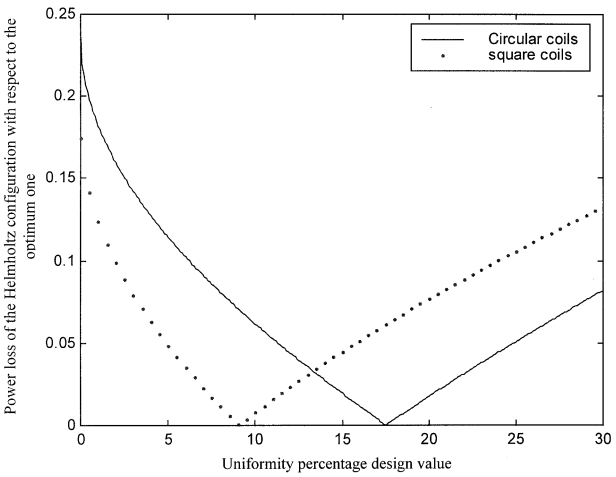

Fig. 9. Power loss of Helmholtz configuration with respect to optimum one versus uniformity design value.

$$P_{si\max} = \frac{\rho_m 4 B_{si\max} I_{is\max}}{s} \frac{\left[\frac{1}{4}\left(\frac{d_s}{a_s}\right)^2 + 1\right]\sqrt{2 + \frac{1}{4}\left(\frac{d_s}{a_s}\right)^2}}{\mathrm{scf}_s^2 \mu_0} r_{tvs}^2. \tag{18b}$$

After some mathematics, for any value of the uniformity percentage error it results that

$$\frac{\left[\frac{1}{4}\left(\frac{d_c}{a_c}\right)^2_{\mathrm{opt}} + 1\right]^{3/2}}{\mathrm{scf}^2_{\mathrm{opt}c}\mu_0} < \frac{\left[\frac{1}{4}\left(\frac{d_c}{a_c}\right)^2 + 1\right]^{3/2}}{\mathrm{scf}_c^2 \mu_0} \tag{19a}$$

$$\frac{\left[\frac{1}{4}\left(\frac{d_s}{a_s}\right)^2_{\mathrm{opt}} + 1\right]\sqrt{2 + \frac{1}{4}\left(\frac{d_s}{a_s}\right)^2_{\mathrm{opt}}}}{\mathrm{scf}^2_{\mathrm{opt}s}\mu_0} < \frac{\left[\frac{1}{4}\left(\frac{d_s}{a_s}\right)^2 + 1\right]\sqrt{2 + \frac{1}{4}\left(\frac{d_s}{a_s}\right)^2}}{\mathrm{scf}_s^2 \mu_0}. \tag{19b}$$

As a consequence, with respect to any other possible configuration, the optimum configuration minimizes the maximum power consumption. Fig. 9 shows the behavior of the percentile difference in the maximum power consumption between the optimum configuration and the Helmholtz one versus the uniformity percentage design value, the test volume being equal. In particular, with respect to the Helmholtz configuration, for a 1% uniformity value the power saving is about 22% in the case of circular coils, and about 15% in the case of square coils, the test volume being equal.

IV. CONFIGURATION BASED ON MORE COILS PER AXIS

If two couples of coils per axis are considered, the modulus percentage error is given by the following analytical expression:

$$\begin{aligned} e_{M12} &= \frac{B_{1\mathrm{nom}} + B_{2\mathrm{nom}} - B_1 - B_2}{B_{1\mathrm{nom}} + B_{2\mathrm{nom}}} \cdot 100 \\ &= \frac{B_{1\mathrm{nom}}}{B_{1\mathrm{nom}} + B_{2\mathrm{nom}}} e_{1M} + \frac{B_{2\mathrm{nom}}}{B_{1\mathrm{nom}} + B_{2\mathrm{nom}}} e_{2M} \end{aligned} \tag{20}$$

where the subscripts 1 and 2 indicate first and second couple of coils, respectively.

The following results from the analysis of 20:

1) If the same configuration is used for the two pair of coils (i.e., they produce test volumes of equal dimensions), the test volume of the four-coil system is equal to the one of a single pair of coils, independent of the amount of the total field generated by each couple of coils.

2) If two different geometrical configurations are used for the two couples of coils (i.e., they produce test volumes of different dimensions), the total test volume dimensions are between the smallest and the largest test volume, depending on the amount of the total field produced by each couple of coils. Of course, in this case, the total test volume is smaller than the one given by the couple of coils that produces the largest test volume. As a result, the analysis of a system of two-couple of coils per axis is restricted to the case in which the two couples of coils have the same geometrical configuration (i.e., they produce test volumes of equal dimensions).

From (17a) and (17b) it follows that the maximum total power consumption of a system of two-couples of coils is given by

$$\begin{aligned} P_{i\max 12} &= P_{i\max 1} + P_{i\max 2} \\ &= [a_1 G_1 \alpha_B \alpha_I + a_2 G_2 (1 - \alpha_B)(1 - \alpha_I)] \\ &\quad \times \frac{\rho_m B_{i\max} I_{i\max}}{s} \mathrm{sf} \end{aligned} \tag{21}$$

where the numerical value of sf (coil shape factor) is 4π for circular coils and 16 for square coils. In the previous equation the subscript i indicates the simulator ith axis, α_B is the percentage of the total maximum field produced by the first couple of coils and α_I is the percentage of the total maximum current flowing into its windings.

It is possible to see that the maximum power consumption is minimized for

$$\alpha_B = \alpha_I = \frac{a_2 G_2}{a_1 G_1 + a_2 G_2}. \tag{22}$$

Combining (21) and (22) it follows that the minimum value of the maximum power consumption is given

by

$$[P_{i\max 12}]_{\min} = \frac{\rho_m a_1 G_1 a_2 G_2 B_{i\max} I_{i\max}}{s(a_1 G_1 + a_2 G_2)}\mathrm{sf}. \tag{23}$$

Of course, it results that

$$\begin{aligned} [P_{i\max 12}]_{\min} &< \frac{\rho_m a_1 G_1 B_{i\max} I_{i\max}}{s}\mathrm{sf} \qquad \text{and} \\ [P_{\max 12}]_{\min} &< \frac{\rho_m a_2 G_2 B_{i\max} I_{i\max}}{s}\mathrm{sf}. \end{aligned} \tag{24}$$

Equation (24) states that the maximum power consumption of the four-coil system, given by (23), is lower than the maximum power consumption of a system consisting of a single pair of coils per axis in the configuration 1 or 2, the maximum field and current being equal.

If the second configuration is more efficient than the first one, in terms of power consumption (i.e., $a_1 G_1 > a_2 G_2$), it results that

$$[P_{i\max 22}]_{\min} \le [P_{i\max 12}]_{\min} \le [P_{i\max 11}]_{\min} \tag{25}$$

where $[P_{i\max 11}]_{\min}$ and $[P_{i\max 22}]_{\min}$ are the minimum values of the maximum power consumption of a four-coil system with the two couples of coils in the configuration 1 and 2, respectively.

As a consequence, the best configuration for the four-coil system is the one in which two optimum configurations, with the same test volume dimensions, are used for the two couples of coils. This means that coils of equal dimensions are used both in the case of circular and square coils. Of course this kind of system is equivalent to a two-coil system, in the optimum configuration, with two parallel-connected coils mounted on the same structure and with a number of windings equal to the one given by (13a) or (13b). As a results, the maximum current is halved, whereas the number of windings per coil is doubled. This allows a consistent power savings (50%), but, according to (15a) and (15b), it doubles the error in the nominal field, the supply current standard deviation being equal.

V. COMPARISON BETWEEN THE CIRCULAR COIL SYSTEM AND THE SQUARE COIL SYSTEM

Considering the two simulator classes, in order to find the best system configuration a comparison between the two optimum configurations based on the use of circular and square coils is performed by using the maximum power consumption and the test volume dimension as parameters. From (18a) and (18b), it follows that

$$\frac{P_{si\max}}{P_{ci\max}} = \frac{\left[\frac{1}{4}\left(\frac{d_s}{a_s}\right)^2_{\mathrm{opt}} + 1\right]\sqrt{2 + \frac{1}{4}\left(\frac{d_s}{a_s}\right)^2_{\mathrm{opt}}}\, r_{tvs}^2 \mathrm{scf}_c^2 B_{si\max} I_{si\max}}{\pi \mathrm{scf}_s^2 r_{tvc}^2 \left[\frac{1}{4}\left(\frac{d_c}{a_c}\right)^2_{\mathrm{opt}} + 1\right]^{3/2} B_{si\max} I_{si\max}}. \tag{26}$$

Therefore, from the comparison between the maximum power consumptions (maximum magnetic field, test volume dimension and maximum supply current being equal) it results that

$$\frac{P_{si\max}}{P_{ci\max}} = \frac{1}{\pi}\frac{\left[\frac{1}{4}\left(\frac{d_s}{a_s}\right)^2_{\mathrm{opt}} + 1\right]\sqrt{2 + \frac{1}{4}\left(\frac{d_s}{a_s}\right)^2_{\mathrm{opt}}}}{\mathrm{scf}_s^2} \times \frac{\mathrm{scf}_c^2}{\left[\frac{1}{4}\left(\frac{d_c}{a_c}\right)^2_{\mathrm{opt}} + 1\right]^{3/2}}. \tag{27}$$

On the other hand, substituting (11a) and (11b) into (13a) and (13b) and considering (17a) and (17b) it follows that

$$\frac{a_s}{a_c} = \sqrt{\frac{P_{si\max}}{I_{si\max}} \frac{1}{\left[\frac{1}{4}\left(\frac{d_s}{a_s}\right)^2_{\mathrm{opt}} + 1\right]\sqrt{2 + \frac{1}{4}\left(\frac{d_s}{a_s}\right)^2_{\mathrm{opt}}}\, B_{si\max}} \frac{\pi I_{ci\max}}{P_{ci\max}} \left[\frac{1}{4}\left(\frac{d_c}{a_c}\right)^2_{\mathrm{opt}} + 1\right]^{3/2} B_{ci\max}}. \tag{28}$$

If the test volume dimensions are now compared (maximum magnetic field, maximum power consumption and maximum supply current being equal), considering (28), it follows that

$$\frac{r_{tvs}}{r_{tvc}} = \frac{\mathrm{scf}_s a_s}{\mathrm{scf}_c a_c} = \sqrt{\pi \frac{\mathrm{scf}_s^2}{\left[\frac{1}{4}\left(\frac{d_s}{a_s}\right)^2_{\mathrm{opt}} + 1\right]\sqrt{2 + \frac{1}{4}\left(\frac{d_s}{a_s}\right)^2_{\mathrm{opt}}}} \frac{\left[\frac{1}{4}\left(\frac{d_c}{a_c}\right)^2_{\mathrm{opt}} + 1\right]^{3/2}}{\mathrm{scf}_c^2}}. \tag{29}$$

By comparison of (27) and (29) it results that the best solution in terms of power consumption is the best solution also in terms of test volume dimensions. Figs. 10(a) and (b) show the behavior of the ratios $P_{s\max}/P_{c\max}$ and r_{tvs}/r_{tvc} versus the uniformity

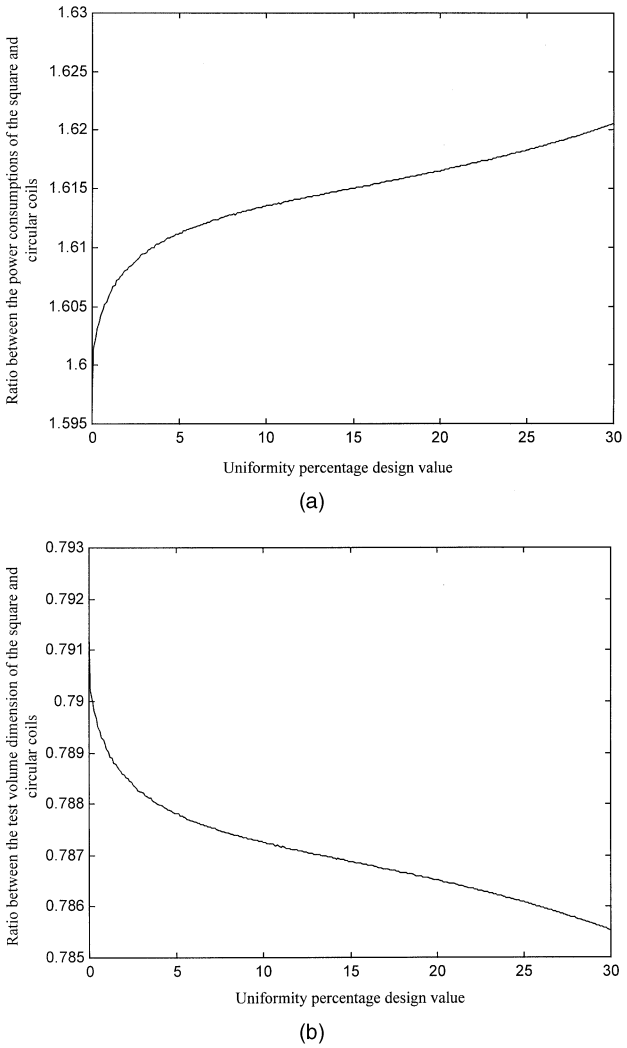

Fig. 10. Comparison between circular and square coils.

percentage design value. From Figs. 10(a) and 10(b) it can be observed that the best solution in terms of both power consumption and test volume dimensions is to use circular coils.

VI. CONCLUSIONS

In this paper, design criteria of a magnetic field simulator for space applications have been presented. In particular, two simulator classes have been considered: high intensity field and high uniformity field simulators. In order to find the simulator geometrical configuration which best realizes the above two classes, different solutions, in terms of coil number, shape, dimension and distance, have been analyzed. In particular, two coil shapes have been considered: circular and square coils. To this end, analytical and numerical models based on a two-coil system have been used.

The analytical and numerical study has demonstrated that, for any field uniformity design value, an optimum geometrical configuration can be found that realizes the following objectives:

1) maximization of the test volume dimension in which a predetermined value of the field uniformity is realized, for given coil dimensions.

2) minimization of the maximum electrical power consumption, the test volume being equal.

The following have also been demonstrated:

1) The use of the optimum configuration has no effects on the nominal field accuracy, this last one depending only on the maximum value of the magnetic field to be simulated and on the maximum value and standard deviation of the coil supply current.

2) No benefits, in terms of uniformity volume dimensions, can be introduced by adding more than two coils per axis, although this allows the maximum power consumption to be lowered, at the cost of reducing the magnetic field accuracy.

Finally, by a comparison between the circular-coil and square-coil based configurations, it has been demonstrated that, for both the two simulator classes, circular coils represent the best solution in terms of maximum power consumption and ratio between test volume and coil dimensions.

ACKNOWLEDGMENTS

This work was supported by the Italian Space Agency, the Ministry for University and Scientific and Technological Research, and Regione Campania.

REFERENCES

[1] D'Errico, M., and Vetrella, S. (1997)
Mission analysis of an Earth observation microsatellite.
Presented at the 48th International Astronautical Congress, Oct. 6–10, Turin, Italy, 1997; Paper IAF-97-B.3.01.

[2] Billingsley magnetics data sheet (1996)
http://www.magnetometer.com.

[3] Meda, Inc. data sheet (1998)
http://www.meda.com.

[4] Feynman, R. P., Leighton, R. B., and Sands, M. (1963)
The Feynman Lectures on Physics, vol. II.
Reading, MA: Addison-Wesley, 1963.

[5] Halliday, D., and Resnick, R. (1996)
Physics—Part II.
New York: Wiley, 1996.

[6] Wertz, J. R. (Ed.) (1978)
Spacecraft Attitude Determination and Control.
Boston: D. Reidel Publishing Company, 1978.

[7] Bevington, P. R. (1969)
Data Reduction and Error Analysis for the Physical Sciences.
New York: McGraw-Hill, 1969, 56–65.

Massimiliano Pastena was born in Naples on October 3, 1970. He received the doctoral degree in aeronautics engineering in 1995. In 1999 he received the Ph.D. in space science and technology.

His research activity covers the dynamics and control of aerospace systems, the design and development of microsatellites and of laboratory facilities for microsatellite ground testing.

Dr. Pastena has published in distinguished journals such as *Journal of Guidance, Control and Dynamics*, *Journal of the Astronautical Sciences*, *Acta Astronautica*, and conference proceedings.

Michele Grassi was born in Naples on April 19, 1963. He received the doctoral degree in aeronautics engineering in 1989. In 1994 he received the Ph.D. in aerospace engineering.

Since 1998 he has been an Associate Professor of Aerospace Systems at the University of Naples "Federico II." His research activity covers the dynamics and control of aerospace systems, the design of space systems for remote sensing applications, the design and development of microsatellites and of laboratory facilities for space system ground testing.

Dr. Grassi has published in distinguished journals such as *Journal of Guidance, Control and Dynamics*, *Journal of the Astronautical Sciences*, *Acta Astronautica*, *Journal of Spacecraft and Rockets*, and conference proceedings.